



1 **Comparative Analysis of MODIS, MISR and AERONET Climatology**
2 **over the Middle East and North Africa**

3 **Ashraf Farahat**

4 Department of Physics, King Fahd University of Petroleum and Minerals, Dhahran 31261,
5 Saudi Arabia;
6 E-Mails: farahata@kfupm.edu.sa

7 *Author to whom correspondence should be addressed; E-Mail: farahata@kfupm.edu.sa.
8 Tel: (321) 541-7088

9

10 **Abstract:**

11 Comparative analysis of MISR MODIS, and AERONET AOD products is performed over
12 seven AERONET stations located in the Middle East and North Africa for the period of
13 2000 – 2015. Sites are categorized into dust, biomass burning and mixed. MISR and
14 MODIS AOD agree during high dust seasons but MODIS tends to underestimate AOD
15 during low dust seasons. Over dust dominated sites, MODIS/Terra AOD indicate a
16 negative trend over the time series, while MODIS/Aqua, MISR, and AERONET depict a
17 positive trend. A deviation between MODIS/Aqua and MODIS/Terra was observed
18 regardless of the geographic location and data sampling. The performance of MODIS is
19 similar over the entire region with ~68% of AOD within the $\Delta\tau = \pm 0.05 \pm 0.15\tau_{AERO}$
20 confidence range. MISR AOD retrievals fall within 72% of the same confidence range for
21 all sites examined here. Both MISR and MODIS capture aerosol climatology; however few
22 cases were observed where one of the two sensors better captures the climatology over a
23 certain location or AOD range than the other sensor.

24 **Keywords:** AOD; Remote Sensing; North Africa; Middle East; Validation

25

26

27



28 **1. Introduction**

29 The Middle East and North Africa host the largest dust source in the world, the Sahara
30 Desert in North Africa that may be responsible for up to 18 percent of global dust emission
31 (Todd et al., 2007, Bou Karam et al. 2010, Schepanski et al. 2016). The vast 650,000 km²
32 Rub' al Khali (Empty Quarter) sand desert is a major source of frequent dust outbreaks and
33 severe dust storms that has major effect on human activity in the Arabian Peninsula (Böer,
34 1997, Elagib and Addin 1997, Farahat et al., 2015).

35 Air quality over the Arabian Peninsula has received significant attention during the past 15
36 years due to *unprecedented overall economic growth, and a booming oil and gas industry,*
37 *however, air pollution studies are still far from complete.* Frequently blowing dust storms
38 play a significant role in pollutant transport over the Arabian Peninsula; and major
39 environmental pollution events such as burning of Kuwait oil fields during the 1991, Gulf
40 War resulted in a large environmental impact on the Arabian Gulf Area (Sadiq and
41 McCain, 1993, and Farahat 2016).

42 Aerosol optical depth, AOD, (also called aerosol optical thickness, AOT) as a parameter
43 indicates the extinction of a beam of radiation as it passes through a layer of atmosphere
44 that contains aerosols. Both satellites and ground-based instruments can be used to measure
45 AOD in the atmosphere, but within the same temporal coordinates and geographic location
46 different instruments could generate different retrievals (Kahn et al., 2007, Kokhanovsky et
47 al., 2007, Liu et al., 2008 and Mishchenko et al., 2009).

48 Since the turn of the 21st century, an upward trend of remotely sensed and ground-based
49 AOD and air pollutants was observed over the Middle East and North Africa (El-Askary
50 2009, Ansmann et al. 2011, Yu et al. 2013, Chin et al. 2014, Yu et al. 2015, Farahat et al.
51 2016, Solomos et al. 2017). This positive trend is attributed to the increase in the Middle
52 Eastern dust activity (Hsu et al., 2012) due to changes in wind speed and soil moisture
53 (Ginoux et al. 2001 and Kim et al. 2013). Yu et al., (2015) concluded that the persistent La



54 Niña conditions (Hoell et al., 2013) have caused increment in Saudi Arabian dust activity
55 during 2008 – 2012. Energy subsidies also encourages energy overconsumption in the
56 Middle East and North Africa with little incentive to adopt cleaner technology. Lack of
57 applying strict environmental regulations have permitted exacerbated urban air pollution.
58 During the last two decades, a large number of satellites, ground stations and computational
59 models contributed to build global and regional maps for the temporal and spatial aerosol
60 distributions. While, ground-based stations and field measurements can identify aerosols
61 properties over specific geographic locations, the sparse and non-continues data from
62 ground-based sensors scattered over the Middle East and North Africa is not sufficient to
63 provide information on spatial and temporal trends of particulate pollution. On the other
64 hand, satellites imagery could provide a significant source of data mapping over larger
65 areas.

66 For its wide spatial and temporal data availability space-born sensors are important sources
67 to understand aerosols characteristics and transport, however low sensitivity to particle type
68 under some physical conditions, high surface reflectivity, persistent cloud, and generally
69 low aerosol optical depth could limit satellite data application in characterizing properties
70 of airborne particles, especially in the Middle East.

71 In order to evaluate the efficiency of space-borne sensors in representing ground observations
72 recorded by AERONET stations we have performed detailed statistical inter-comparison
73 analysis between satellite AOD products and AERONET for seven stations in the Middle East
74 and North Africa representative for dust, biomass burning, and mixed aerosol conditions
75 (Dubovik et al., (2000, 2002, 2006), Holben et al. (2001), Derimian et al., (2006), Basart et
76 al. (2009), Eck el. (2010), Marey et al., 2010, Abdi et al., (2012)). Previously we analysed
77 these seven AERONET stations to understand particles categorization and absorption
78 properties (Farahat et al. 2016), and the current study extends the analysis to the satellite
79 datasets.



80 In the first part of this article, we validated MISR and MODIS retrievals against collocated
81 AERONET observations. We also assessed the consistency in aerosol trends between
82 space-borne sensors and ground-based data.

83 In the second part, we evaluated representativeness of satellite-derived aerosol climatology
84 over the study region from the long-term AERONET data for MISR and MODIS AOD
85 products. It is especially relevant for the MISR instrument, as its sampling is limited by
86 once per week observations of the same region from the two overlapping paths. MODIS
87 provides nearly daily observations to the same geographic location; however, the quality of
88 the product diminishes over the bright targets potentially affecting MODIS-derived aerosol
89 climatology.

90 The collocated MISR, MODIS and AERONET data were obtained at the MAPSS website
91 (<http://giovanni.gsfc.nasa.gov/mapss.html>).

92

93 **2. Materials and Methods**

94 **2.1 MISR**

95 The Multi-angle Imaging SpectroRadiometer (MISR) instrument to measures tropospheric
96 aerosol characteristics through the acquisition of global multi-angle imagery on the
97 daylight side of Earth. MISR applies nine Charge Coupled Devices (CCDs), each with 4
98 independent line arrays positioned at nine view angles spread out at nadir, 26.1°, 45.6°,
99 60.0°, and 70.5°. In each of the nine MISR cameras, images are obtained from reflected and
100 scattered sunlight in 4 bands blue, green, red, and near-infrared with a centre wavelength
101 value of 446, 558, 672, and 867 nm respectively. The combination of viewing cameras and
102 spectral wavelengths enables MISR to retrieve aerosols AOD over high reflection surfaces
103 like deserts.

104 In this study, we use Level 2 (ver. 0022) AOD at 558 nm (green band) measured by MISR
105 instrument with a 17.6 km resolution aboard the Terra satellite. MISR Level 2 aerosol



106 retrievals use only data that pass angle-to-angle smoothness and spatial correlation tests
107 (Martonchik et al. 2002), as well as stereoscopically derived cloud masks and adaptive
108 cloud-screening brightness thresholds (Zhao and Di Girolamo, 2004).

109 **2.2 MODIS**

110 The Moderate Resolution Imaging Spectroradiometer (MODIS) is a payload instrument on
111 board the Terra and Aqua satellites. Terra's and Aqua orbit around the Earth from North to
112 South and South to North across the equator during the morning and afternoon respectively
113 (Kaufman et al., 1997). Terra MODIS and Aqua MODIS provides nearly daily coverage of
114 the Earth's surface and atmosphere in 36 wavelength bands, ranging from 0.412 to 41.2
115 μm , with spatial resolutions of 250 m (bands 1-2), 500 m (bands 3-7), 1000 m (bands 8-
116 36). Located near-polar orbit (705 km), MODIS has swath dimensions of 2330 km \times 10 km
117 and a scan rate of 20.3 rpm. With its high radiometric sensitivity and swath resolution
118 MODIS retrievals provides information about aerosols optical and physical characteristics.
119 MODIS uses 14 spectral band radiance values to evaluate atmospheric contamination and
120 determine whether scenes are affected by cloud shadow (Ackerman et al., 1998).

121 The MODIS dark-target algorithm is designed aerosol retrieval from MODIS observations,
122 over dark land surfaces (low values of surface reflectance) (e.g., dark soil and vegetated
123 regions) in parts of the visible (VIS, 0.47 and 0.65 μm) and shortwave infrared (SWIR, 2.1
124 μm) spectrum (Kaufman et al., 1997). Level 2 (C006) of the algorithm are used to retrieve
125 MODIS aerosols' time series data. Levy *et al.* (2010) reported that the dark-target
126 algorithm AOD at 550 nm measurement for (C005) includes uncertainty of $\pm (0.05\tau+0.03)$
127 and $\pm (0.15\tau+0.05)$ over ocean and land respectively. This uncertainty is caused by
128 uncertainties in computing cloud masking, surface reflectance, aerosol model type (e.g.,
129 single scattering albedo), pixels selections and instrument calibration.



130 **2.3 AERONET**

131 The Aerosol Robotic Network (AERONET) (Holben et al., 1998 and Holben et al., 2001) is
132 a ground-based remote sensing aerosols network that provides a long-term data related to
133 aerosol optical, microphysical and radiative properties. With over 700 global stations, the
134 AERONET data is widely used in validating satellite retrievals (Chu et al., 1998 and
135 Higurashi et al., 2000).

136 The sun photometers used by AERONET measure spectral direct-beam solar radiation, as
137 well as directional diffuse radiation in the solar almucantar. The former are used to
138 determine columnar spectral AOD and water vapour, provided at a temporal resolution of
139 approximately 10–15 min (Sayer et al. 2014). AERONET direct-sun AOD has a typical
140 uncertainty of 0.01–0.02 (Holben et al., 1998) and is provided at multiple wavelengths at
141 340, 380, 440, 500, 675, 950, and 1020 nm.

142 Seven AERONET sites were selected for satellite validation in this study (Table 1.). The
143 sites were selected based on their geographic locations to represent aerosols characteristics
144 over North Africa and the Middle East (Farahat et al., 2016). A record of long-term data
145 collection was another factor in the selection process.

146 **Data Matching Approach**

147 Multi-sensors data matching requires using only compatible data to eliminate uncertainties
148 associated with cloud shadow and spatial and temporal retrievals produced by different
149 instruments (Liu and Mishchenko (2008) and Mishchenko et al., 2009).

150 The comparison of MISR and MODIS products against AERONET is performed to
151 evaluate satellites' retrieval over individual North Africa and Middle East sites (see Table
152 1). There is only a small number of AERONET measurements that are perfectly collocated
153 with MODIS and MISR. One way to work with this lack of compatibility problem is to
154 compare satellites measurements nearby a certain AERONET site and comparing



155 AERONET measurements nearly synchronized with the satellite overpass time (Sioris et al.
156 2017). Another reasonable strategy is to average all satellite measurements with a certain
157 distance of an AERONET location and average all AERONET measurements within a
158 certain time range (Mishchenko et al., 2010). The results presented in this paper are based
159 on the second approach as it compares average spatial satellite measurements with average
160 temporal AERONET measurements. We implemented the Basart et al., (2009) approach in
161 using a spatial and temporal threshold of 50 km and 30 min for MISR, MODIS, and
162 AERONET data matching.

163 We use the Giovanni Multi-sensor Aerosol Products Sampling System MAPSS
164 (<http://giovanni.gsfc.nasa.gov/aerostat/>) for the data inter-comparison as aerosols products
165 are averaged from measurements that are within a radius of ~ 27.5 km from the AERONET
166 station and within 30 min of each satellite flyover over this location. These data are
167 represented in the article by MISR / MODIS “matched AERONET data”.

168 “All data” represents AOD products at the selected station. AERONET station ‘all data’
169 are obtained through AEROSOL ROBOTIC NETWORK (AERONET) website
170 (<https://aeronet.gsfc.nasa.gov/>). Daily AOD data with level 2.0 quality was used in the
171 analysis (Smirnov et al., 2000) . Level 2.0 AOD retrievals are accurate up to 0.02 for mid-
172 visible wavelengths.

173 MISR ‘all data’ is available through MISR website ([https://www-
174 misr.jpl.nasa.gov/getData/accessData/](https://www-misr.jpl.nasa.gov/getData/accessData/)).

175

176 3. Statistics

177 We have used two statistical parameters to compare data retrievals from space-borne and
178 ground based sensors including:

179 (1) Correlation coefficient (R),



180 The correlation coefficient is a parameter to measure data dependence. If the value of R is
181 close to zero, it indicates weak data agreement. And values close to 1 or -1 indicate that
182 data retrievals are positively or negatively linearly related (Cheng et al., 2012).

183

184 (2) Good Fraction (G- fraction).

185 The G- fraction indicator uses a data confidence range defined by MISR and MODIS
186 (Bruegge et al., 1998 and Remer et al., 2005) over the land and ocean that combines
187 absolute and relative criterion and weights data equally such that small abnormalities will
188 not affect the inter-comparison statistics (Kahn et al., 2009). In this study, we use MODIS
189 confidence range which defines data retrieval as “good” if the difference between MODIS
190 and AERONET is less than

191 $\Delta\tau = \pm 0.03 \pm 0.05\tau_{AER}$, Over ocean, (1)

192 $\Delta\tau = \pm 0.05 \pm 0.15\tau_{AER}$, Over land. (2)

193

194 where τ_{AER} is the optical depth retrieved using AERONET stations. The G-fraction is the
195 percentage of MODIS data retrievals that satisfies (Equations (1) and (2)) over ocean and
196 land respectively. Optical depth threshold over land (Equation (1)) is higher than over
197 ocean (Equation (2)) due to harder data retrievals and high data instability over land.

198 A good aspect of using data confidence range is excluding small fraction data outliers from
199 producing inexplicably large influence on comparison statistics by weighting all events
200 equally.

201

202 4. Results and discussion

203 4.1 Validating MISR and MODIS AOD retrievals against AERONET observations 204 over the Middle East and North Africa



205 Illustrated in Figures 2, 3 and Tables 2, 3 is a regression analysis of MISR and MODIS
206 Terra AOD products against AERONET AOD over the seven AERONET sites, shown in
207 Table1, from 2000 – 2015.

208 The correlation coefficient between MISR and AERONET AOD at region 1 is equal to or
209 above 0.85 except in Bahrain during DJF and JJA (Figure (2) and Table 2), which could be
210 attributed to lack of data and the impact of water surface reflectivity over Bahrain. Similar
211 correlation coefficient values were found in region 2 where MISR-AERONET AOD shows
212 less error than MODIS (Figures (2, 3) and Table 3). In general, MODIS-AERONET AOD
213 correlation coefficient is lower than those of MISR at all sites, except Mezaira, where
214 MISR and MODIS matched AERONET AOD correlation almost match. The lowest
215 MODIS-AERONET AOD correlation coefficient was found over Cairo but could be
216 attributed to the lack of data availability at this location (Figs 3e-h). Low values of
217 MODIS-AERONET correlation coefficient is also found over Saada, Taman, and Sedee
218 Boker sites.

219 Over all AERONET stations, the number of MODIS AERONET matched AOD are 4 to 8
220 times those of MISR which is expected from the MISR's sampling.

221 Comparisons show that the difference between MISR and MODIS retrievals at the selected
222 AERONET sites could be significant as expected from the MODIS Dark Target algorithm
223 performance over bright land surfaces Kokhanovsky et al. (2007).

224 High AOD values over regions 1 and 2 measured by both AERONET and satellites'
225 sensors indicate higher dust activities that peaks during May – Aug during dust storms
226 season. Higher AOD values recorded during SON over Cairo station could be caused by
227 seasonal rice straw burning by farmers in Cairo, an environmental phenomena known as
228 Cairo Black cloud (Marey et al. 2010). As shown in (Figure (3)), the daily variability in
229 MODIS measurements is larger than those of MISR at all the three regions. In general,



230 MODIS tends to underestimate the AOD values on low dust seasons (Figures (2, 3) and
231 Tables 2, 3).

232 The MODIS underestimated AOD values are more noticeable over Bahrain. This could be
233 attributed to large water body surrounding Bahrain, which should affect surface reflectivity.
234 Moreover, water in the Arabian Gulf has been polluted in recent years (Afnan 2013),
235 leading to possible changes in watercolour and uncertainties in calculating surface
236 reflectivity. The patchy land surface or pixel grid contaminated by water body is the
237 dominant error sources for MODIS aerosol inversion over the land areas (He et al. 2010).

238 Compared to MODIS, MISR's outperform in retrieving AOD over region 1 including vast
239 highly reflecting desert areas can be attributed to its multispectral and multi-angular
240 coverage, which make MISR provide better viewing over a variety of landscapes.
241 Meanwhile, MISR retrieval also takes into consideration aerosols' particles nonsphericity,
242 which could have significant effect on its AOD retrievals (von Hoyningen-Huen and Posse
243 1997). MISR's retrieval did not perform well over Cairo site due to lack of matched points
244 in most of the seasons (13 in DJF, 5 in MAM & JJA, and 4 in SON during 2000 - 2015).

245

246 **4.2 Trends of AOD MISR, MODIS, and AERONET retrievals over the Middle East** 247 **and North Africa**

248 Figure 4 shows time series of monthly mean AOD derived from MODIS/Aqua,
249 MODIS/Terra, MISR and AERONET over a) dust b) biomass and c) mixed dominated
250 aerosol regions. The satellite AOD trends are calculated from the data collocated with
251 AERONET observations.

252 MODIS/ Aqua and MISR AOD at Solar Village have positive trends, while MODIS/ Terra
253 AOD have negative trends along time series (Fig. 4a). MODIS-Aqua AOD differ from
254 those of MODIS-Terra. Discrepancy between Aqua and Terra retrievals could be related to



255 instrument calibration, or the difference in aerosol and cloud conditions from the morning
256 to the afternoon. Both MODIS Aqua and Terra are underestimating AOD at Solar Village.
257 MISR AOD trend shows a better agreement with Solar Village AERONET AOD as
258 compared to MODIS.

259 Both MODIS/Aqua and MODIS/Terra AOD show a stable trend over time at Mezaria site
260 with a correlation coefficient of 0.11 and 0.04 respectively. MODIS/Aqua AOD over
261 Bahrain (not shown in the figure) show, less time trend stability compared to those at Solar
262 Village with a correlation coefficient 0.63. MODIS/Aqua, MODIS/Terra, and MISR AOD
263 depicts a positive trend over Cairo, however a 2 years of available AERONET data is not
264 sufficient for the trend analysis (Fig. 4b). Taman site (Fig. 4c): MODIS/Aqua, MODIS/
265 Terra, MISR AOD agrees with Taman AERONET on a negative trend indicating data
266 stability over this site.

267 Long-range (2000 – 2015) tendency indicates that contradictory AOD trend of Terra and
268 Aqua is site-dependent and does not necessarily apply everywhere.

269 AOD difference between Terra and Aqua could be used as another indicator of the long-
270 range satellites performance. AOD difference (Terra AOD minus Aqua AOD) varies from -
271 0.01 to 0.19, -0.10 to 0.18, -0.02 to 0.13 over Solar Village, Taman, and Cairo respectively
272 (Fig. 5). Over the Solar Village, Terra overestimates AOD during 2002-2004 and
273 underestimates the AOD after 2005. Although Cairo and Taman show similar trend
274 however over/underestimation amount is not unique for all sites. This is an indication that
275 Aqua and Terra retrievals disagreement takes place regardless of the region but site
276 sampling has significant effect on the amount of contradiction.

277 Statistical comparison between MISR and MODIS/Terra AOD at corresponding
278 AERONET stations is performed by calculating G-fraction using of $\Delta\tau = \pm 0.05 \pm 0.15\tau_{AERO}$
279 as a confidence interval. Over the region 1, MISR AOD retrievals are more accurate than



280 MODIS retrievals. MODIS, however, performs better over region 2 sites with high
281 percentage of the data points falling within the confidence range (Tables 2 and 3). High
282 light reflections from the desert landscape surrounding region 1 could have an effect on
283 MODIS retrievals.

284 Excluding Bahrain and Cairo for low data retrievals the performance of MODIS tends to be
285 similar over all region with ~ 68 percent of AOD retrievals fall within the
286 $\Delta\tau = \pm 0.05 \pm 0.15\tau_{AERO}$ confidence range of the AERONET AOD while MISR retrievals
287 show better performance with ~ 72 percent of the data falling within the same confidence
288 range. This could be attributed to low number of retrievals available for Bahrain and Cairo
289 compared to other sites. Vast sea region surrounding Bahrain and complex landscape in
290 Cairo could also have an impact on retrievals.

291 **4.3 Evaluating the MISR and MODIS climatology over Middle East and North Africa**

292 Comparisons between MISR and MODIS AOD at selected AERONET stations over the
293 2000 – 2015 period are illustrated in Figures 6- 12.

294 Figure (6a, b) shows histogram of the MISR, MODIS and AERONET AOD at Solar
295 Village for MISR and MODIS data points collocated with AERONET observations. The
296 mean, standard deviation, and number of measurements are also presented.

297 MISR tends to underestimate the frequency of low AOD compared to AERONET but
298 overestimate the frequency of high AOD. MISR histograms show prominent peaks at 0.55
299 and 0.75 not seen in AERONET. MISR and AERONET AOD climatology agree well with
300 one another. MODIS also tends to underestimate the frequency of low AOD events and
301 overestimate the frequency of high AOD events. High surface reflectance could cause
302 overestimation in MODIS AOD (Ichoku et al., 2005). Both MISR and MODIS provide a
303 good representation of the AOD climatology as compared to AERONET at the Solar
304 Village. Mezaria station, which is located in an arid region in the UAE, has a similar



305 climatology to the Solar Village site with dust dominating aerosol. Figure (7a, b) shows
306 histograms of the MISR, MODIS and AERONET AOD at Mezaria.
307 Unlike Solar Village, there is a big difference between the number of samples in the
308 matched data set and full AERONET climatology. For MISR there are 116 matched cases
309 and for MODIS there are 498 compared to the 1517 for the entire site. This has an impact
310 on the overall assessment showing significant differences between the matched data and the
311 full climatology for both MISR and MODIS. First, for the MISR case, the matched
312 AERONET data have the highest frequency at AOD of 0.3 and 0.35, but the climatology
313 shows the highest frequency at an AOD of 0.25. Second AOD in the range of 0.3 to 0.45
314 are oversampled relative to the climatology, and AOD less than 0.3 and greater than 0.5 are
315 under-sampled with no AOD greater than 0.8. MODIS matched AERONET data show
316 prominent peaks at 0.3 and 0.4 compared to the climatology that has a single peak at 0.25.
317 For AOD values between 0.3 and 0.6 MODIS data were found to be under-sampled similar
318 to MISR AOD.
319 MISR AOD retrievals matched to AERONET capture the variability in the distribution, but
320 as in the case of Solar Village the frequency of low AOD events is underestimated and the
321 frequency of high AOD events is overestimated. However, MISR does capture events with
322 AOD greater than 1. A similar situation is seen in the MODIS comparison, but MODIS
323 appears to do a better job capturing the overall shape of the AERONET AOD histogram for
324 this site.
325 The Bahrain AERONET site is located in Manama fairly close to the Arabian Gulf, a
326 location very different from the previous two sites. The site is also located in an urban area
327 suffers from significant load of anthropogenic aerosols as a consequence of rapid
328 aluminium industrial development (Farahat 2016). Figure (8a, b) shows histogram of the
329 MISR, MODIS and Bahrian AERONET measurements with statistical analysis displayed.



330 The AERONET data matched to MISR show significant peaks at 0.25, 0.35, and 0.5 not
331 seen in the all data climatology that has a single peak at 0.35. AOD less than 0.25 and
332 greater than 0.6 are not representative in the matched data set at all. MISR is representing
333 the peaks at 0.25 and 0.35 in the matched data set but misses the peak at 0.5. The MISR
334 climatology agrees well with the AERONET all data climatology for all AOD. MODIS on
335 the other hand shows an extremely large frequency of AOD at 0.1 not represented by
336 AERONET coupled with an underestimation of AOD greater than 0.3. This could be
337 attributed to the size of the matching window and MODIS retrievals preferentially coming
338 from the Arabian Gulf.

339 SAADA station is located close to some hiking trails at the Agoundis Valley in the Atlas
340 Mountains about 197 km from the city of Marrakesh.

341 MISR AOD matched to AERONET agree well with MISR full climatology retrievals over
342 SAADA station. Both retrievals slightly underestimate SAADA full climatology and over
343 estimates SAADA matched data retrievals at AOD equal to 0.1 while show good agreement
344 for AOD greater than 0.1. MODIS matched to AERONET retrievals overestimate the
345 frequency of AOD greater than 0.3. While MODIS AOD matched to AERONET captures
346 climatology at AOD between 0.2 to 0.25, AOD frequency retrievals are under-sampled at
347 AOD between 0.1 to 0.15 with about 13 % less events than SAADA all data retrievals at
348 AOD equal to 0.1.

349 Figure (9a, b) indicates right skewed distribution of SAADA AOD towards small AOD
350 values with 11.5 % and 30.1 % of AOD > 0.4 as measured by MISR and MODIS
351 respectively. Taking into consideration MODIS overestimation we conclude that SAADA
352 site is characterized by small AOD values and this could be related to the land topology
353 where the station is located.



354 While MISR is capturing high AOD climatology over SAADA, both MISR and MODIS
355 are underestimating the frequency of lower AOD events. Nevertheless, MISR captures the
356 climatology of AOD less than 0.1 missed by MODIS retrievals.

357 Taman AERONET station is located at the oasis city of Tamanrasset, which lies in
358 Ahaggar National Park in southern Algeria.

359 Figure (10 a, b) depicts that Taman AERONET AOD climatology is similar to those at
360 SAADA and has a high frequency of low AOD events. Both MISR AOD matched to
361 AERONET and MISR all data do not well capture the frequency of AOD less than 0.1 or
362 larger than 1 while well describe the climatology for AOD in the range of 0.1 to 1. MODIS
363 AOD matched data to AERONET correctly describe climatology with slight overestimation
364 of AOD frequencies between 0.05 – 0.15 while not capturing AOD frequencies greater than
365 1. MISR and MODIS show similar prominent peaks at 0.1, 0.25, and 0.35, not observed in
366 Taman AERONET AOD climatology, with more peaks observed by MISR at 0.5, 0.6, and
367 0.8. Average AOD in SAADA and Taman is ~ 50 percent less than observed at Solar
368 Village, Mezaria, and Bahrain sites.

369 Except for AOD greater than 1 where ground observations could be more robust, both
370 MISR and MODIS retrievals can provide very good climatology matching over Taman site.
371 Taking into consideration lower number of MISR matching AERONET observations
372 compared to MODIS ~ 33 and 43 percent over SAADA and Taman respectively, MISR is
373 outperforming over these two sites which can be attributed to its multiangle viewing
374 capabilities over complex terrains including mountainous areas (Atlas Mountains).

375 Cairo is a mega city well known for its high pollution due to traffic and agriculture
376 activities.

377 MISR and MODIS matched data correctly capture AOD climatology over Cairo compared
378 to AERONET as shown in Figure (11a, b). MISR retrievals collocated with AERONET



379 capture prominent peaks of AERONET AOD at 0.15 – 0.25 and 0.5 with small
380 underestimation observed at 0.3. MISR ‘all data’ AOD climatology over Cairo station
381 agrees better with AERONET AOD climatology vs. collocated dataset with some
382 oversampling at 0.15. Frequency of high AOD retrievals at 0.7 and 0.8 have not been
383 captured by MISR matched or all data retrievals. MODIS matched to AERONET AOD are
384 also able to well present Cairo climatology data with a high overestimation of AOD
385 frequency between 0.05 - 0.2 and an underestimation of AOD larger than 0.4.

386 The complex landscape and local emissions in Cairo could impose major challenges in
387 MODIS AOD retrievals. Moreover, Cairo is one of the most densely populated cities in the
388 world that hosts major commercial and industrial centers in North Africa. Cairo also has
389 complicated aerosols structure developed by long range transported dust in the spring,
390 biomass burning in the fall, strong traffic and industrial emissions (Marey et al., 2010).

391 Over Cairo station, MODIS correctly represents ground observations for AOD between 0.2
392 - 0.4 while MISR all data better represents AOD climatology for AOD greater than 0.4.
393 There is not enough collocated MISR-AERONET AOD to evaluate MISR ‘matched AOD’
394 climatology.

395 MISR, MODIS climatology at SEDEE Boker are illustrated in Figures (12a, b).

396 MISR ‘matched’ AOD frequency show significant underestimation for AOD less than 0.2
397 and an overestimation between 0.2 – 0.4 compared with AERONET retrievals. MISR
398 correctly captures the climatology for AOD events greater than 0.4. MISR ‘matched’ and
399 ‘all data’ retrievals peaks at 0.25 and 0.2 respectively producing high frequency of AOD
400 oversampling compared to AERONET. MISR data retrievals do not capture the
401 climatology for AOD less than 0.1 over this site coincident with what was previously
402 observed over other sites. MODIS matched AERONET data underestimates frequency of
403 AOD less than 0.2 while overestimates the frequencies between 0.2 - 0.6, and well match



404 frequencies of higher AOD events larger than 0.6. MODIS retrievals are characterized by
405 two prominent peaks at 0.1 and 0.25 that are not found in the AERONET matched data.
406 At Sedee, MISR and MODIS retrievals are better in matching frequency of high AOD
407 retrievals (greater than 0.4) than the frequency of low AOD. This could be an effect of
408 possible long-range transport to Sedee Boker site (Farahat et al. 2016) along with complex
409 mixtures of dust, pollution, smoke, and sea salt that could result in uncertainties in MISR
410 and MODIS aerosol model selection.

411 In the summary, MISR tends to underestimate AOD > 0.4 over Solar Village, Mezaria,
412 Bahrain, and Cairo while agrees with AERONET over SAADA, Taman and Sedee Boker
413 at all ranges of AOD. This could be expounded by insufficient particle absorption in MISR
414 V22 algorithm (Kahn et al., 2005). Spherical particle absorption is produced by externally
415 mixing small black carbon particles.

416 Percentage of MISR, MODIS, and AERONET AOD greater than 0.4 recorded is shown in
417 Table 4. Over Solar Village, both MISR and MODIS well capture high AOD greater than
418 0.4 with very good agreement with the ground observations. Over Mezaria, both MISR and
419 MODIS are over estimating the percentage of AOD greater than 0.4 by about 15.5 and 10.5
420 percent respectively. MISR all data agrees well with AERONET all data in representing
421 high AOD over Bahrain while MODIS shows significant under-representation of those
422 events by about 15 percent, less than reported by Bahrain AERONET station. At SAADA,
423 MISR AOD agrees with AERONET in showing low percentage of AOD greater than 0.4,
424 while MODIS retrievals overestimate percentage by about 24 percent. MISR AOD over
425 Taman AERONET station shows very good agreement, while MODIS is slightly
426 overestimating AOD. Among all seven sites considered in this study, Sedee Boker shows
427 lowest occurrence of AOD greater than 0.4, which is confirmed by both MISR and MODIS



428 retrievals. Cairo AERONET records the highest frequency of AOD > 0.4, however this is
429 largely underestimated by both MISR and MODIS retrievals.

430 It can concluded from the previous discussion that atmosphere around SAADA, Taman,
431 and Sedee Boker sites is relatively clean and aerosol loads are small compared to Solar
432 Village, Mezaria, Bahrain, and Cairo, however this could be affected by the location where
433 AERONET station is installed for example SAADA and Taman stations are installed in a
434 remote mountainous region away from urbanization while Cairo station is installed in the
435 middle of large residential region with significant local emissions.

436

437 **Conclusion**

438 The performance of MODIS, MISR retrievals with corresponding AERONET
439 measurements over different geographic locations in the Middle East and North Africa was
440 investigated during 2000 – 2015.

441 Long-range observations show dissimilar AOD trends between MODIS/Aqua,
442 MODIS/Terra, MISR and AERONET measurements. MODIS/Aqua matched AERONET
443 retrievals show stable trend over all sites while, MODIS/Terra matched AERONET
444 retrievals show significant downward trend indicating possible changes in the sensor
445 performance.

446 MISR matched AERONET AOD data depict high correlation compared to
447 AERONET indicating good agreement with ground observations with about 72 percent of
448 AOD retrievals fall within the expected confidence range.

449 Consistency of MODIS and AERONET AOD vary based on the season, study area,
450 and dominant aerosols type with about 68 percent of the retrieved AOD values fall within
451 expected confidence range with the lowest performance over mixed particles regions.



452 Comparing satellites' AOD retrievals with corresponding AERONET
453 measurements show that space-borne data retrievals accuracy can be affected by landscape,
454 topology, and AOD range at which data is retrieved.

455 Few AERONET sites are verified where MISR and MODIS retrievals agree well
456 with ground observations, while other sites only MISR or MODIS could correctly describe
457 the climatology.

458 The AOD range at which MISR or MODIS could correctly describe ground
459 observation is also investigated over different AERONET sites. Over Solar Village both
460 MISR and MODIS tend to underestimate the frequency of low AOD and overestimate the
461 frequency of high AOD compared to AERONET with MISR histograms show prominent
462 peaks at 0.55 and 0.75 not shown in AERONET. MISR can capture the frequency of AOD
463 greater than 1 mostly missed by MODIS. Both MISR and MODIS are found to provide
464 good representation of the AOD climatology over the Solar Village site.

465 Similar to Solar Village, MISR underestimates frequency of lower AOD and
466 overestimate frequencies of high AOD over Mezaria. MISR is able to correctly capture the
467 frequency of AOD greater than 1, while MODIS retrievals are found to better represent the
468 overall climatology. This is due to low number of MISR – matched AERONET retrievals
469 compared to MODIS over this site. Prominent peaks at 0.3 and 0.4 were observed in
470 MODIS matched Mezaria retrievals compared to the climatology, which has a single peak
471 at 0.25.

472 Large water body surrounding Bahrain makes MODIS data preferentially originate
473 from the Arabian Gulf which produces an extremely large frequency of AOD at 0.1 not
474 observed in AERONET measurements paired with an underestimation of AOD greater than
475 0.3. Meanwhile, MISR retrievals agree well with AOD climatology over Bahrain.



476 MISR AOD retrievals slightly underestimate SAADA climatology while show good
477 agreement for AOD greater than 0.1. MODIS retrievals underestimate the frequency of
478 AOD retrievals between 0.1 to 0.15, match climatology at AOD between 0.2 to 0.25, and
479 overestimate the frequency of AOD greater than 0.3. SAADA site is characterized by
480 small frequency of low AOD values and this could be related to the landscape nature
481 surrounding Saada station. MISR is found to be outperforming over Saada and Taman
482 stations which can be attributed to its viewing multispectral and multiangular capabilities
483 over mountainous regions.

484 MISR retrievals well capture prominent peaks of AERONET data at 0.15 to 0.25
485 and 0.5 with small underestimation observed at 0.3 over Cairo. It is recommended to use
486 MISR all data rather than matched data only over Cairo as it is found to do a better job in
487 describing the climatology over this station. MODIS data retrievals are also able to well
488 present Cairo climatology with a high overestimation of AOD frequency between 0.05 to
489 0.2 and an underestimation of AOD larger than 0.4. While both MISR and MODIS well
490 describe climatology over Cairo station, MODIS can correctly represent ground
491 observations between 0.2 to 0.4.

492 Over Sedee Boker both MISR and MODIS retrievals well describe the climatology
493 however they are more successful in matching frequency of high AOD greater than 0.4.

494 Based on analysing frequency of AOD greater than 0.4, it was found that Saada, Taman,
495 and Sedee Boker are having better air quality compared to other sites while Cairo was
496 found to be the most polluted site.

497 Results presented in this study are important in providing a guideline for satellites retrievals
498 end users on which sensor could provide reliable data over certain geographic location and
499 AOD range.



500 Adjacent geographic location and local climate among sites does not always
501 guarantee that same sensor will provide consistent retrievals over all sites. For example,
502 Solar Village, and Bahrain AERONET are surrounded by large desert regions in the and
503 sharing almost similar climatic conditions, but MODIS is found to be more successful in
504 describing climatology over Solar Village than over Bahrain and this could be attributed to
505 different factors related to surface reflection, cloud coverage, and the large water body
506 surrounding Bahrain. Thus in order to decrease data uncertainty, it is important to
507 determine which sensor provides best retrieval over certain geographic location and AOD
508 range.

509

510 **Acknowledgements**

511 The author would like to acknowledge the support provided by the Deanship of Scientific
512 Research (DSR) at the King Fahd University of Petroleum and Minerals (KFUPM) for
513 funding this work through project # IN161053. Portions of this work were performed at the
514 Jet Propulsion Laboratory (JPL), California Institute of Technology, under a contract with
515 the National Aeronautics and Space Administration. The author would like to thank
516 Michael Garay (MJG) and Olga Kalashnikova (OVK) (JPL) for their suggestion of
517 investigating satellites – AERONET matched data climatology, and discussion during the
518 data analysis. The author would also like to thank Hesham El-Askary (Chapman
519 University) for providing recommendation about AERONET data over North Africa and
520 the Middle East as well as reviewing the English in the manuscript. We thank the MISR
521 project for providing facilities, and supporting contributions of MJG and OVK. Finally, we
522 thank the reviewers for suggestions, which improved the manuscript.

523

524

525 **Author Contributions:** Ashraf Farahat analysed the data, performed the statistical analysis
526 and wrote the manuscript.

527

528 **Conflicts of Interest:** The authors declare no conflict of interest.

529

530

531

532

533



534 **References**

- 535 1. Abdi, V., Flamant, C., Cuesta, J., Oolman, L., Flamant, P., and Khalesifard, H. R.
536 Dust transport over Iraq and northwest Iran associated with winter Shamal: A case
537 study. *J. Geophys. Res.*, 117, D03201, 2013.
- 538
539 2. Ackerman, S., Strabala, K. I., Menzel, W. P., Frey, R. A., Moeller, C. C. and
540 Gumley, L. E. (1998): Discriminating clear sky from clouds with MODIS. *J.*
541 *Geophys. Res.*, 103, 32 141–157, 1998.
- 542
543 3. Afnan, F. Heavy metal, trace element and petroleum hydrocarbon pollution in the
544 Arabian Gulf: Review, *Journal of the Association of Arab Universities for Basic*
545 *and Applied Sciences*, 17, 90-100, 2015.
- 546
547 4. Ansmann, A., Petzold, A., Kandler, K., Tegen, I., Wendisch, M., Müller, D.,
548 Weinzierl, B., Müller, T., and Heintzenberg, J. Saharan Mineral Dust Experiments
549 SAMUM-1 and SAMUM-2: what have we learned? *Tellus B*, 63, 403–429, 2011.
- 550
551 5. Basart, S., Pérez, C., Cuevas, E., Baldasano, J. M., and Gobbi, G. P. Aerosol
552 characterization in Northern Africa, Northeastern Atlantic, Mediterranean Basin and
553 Middle East from direct-sun AERONET observations. *Atmos. Chem. Phys.*, 9,
554 8265-8282, 2009.
- 555
556 6. Böer B., An introduction to the climate of the United Arab Emirates (review). *J*
557 *Arid Environ*, 35:3–16, 1997.
- 558
559 7. Bou Karam, D., Flamant, C., Cuesta, J., Pelon, J., and Williams, E. Dust emission
560 and transport associated with a Saharan depression: February 2007 case, *J.*
561 *Geophys. Res.*, 115, D00H27, 2010.
- 562
563 8. Bre'on, F-M., Vermeulen, A., Desclotres, J. An evaluation of satellite aerosol
564 products against sunphotometer measurements. *Remote Sensing Environ.*, 115,
565 3102–11, 2011.
- 566
567 9. Bruegge, C., Chrien, N., Kahn, R., Martonchik, J., and Diner, D. MISR
568 radiometric uncertainty analyses and their utilization within geophysical
569 retrievals. *IEEE Trans. Geosci. Remote Sens.*, 36, 1186- 1198, 1998.
- 570
571
572 10. Chin, M., Diehl, T., Tan, Q., Prospero, J. M., Kahn, R. A., Remer, L. A., Yu, H.,
573 Sayer, A. M., Bian, H., Geogdzhayev, I. V., Holben, B. N., Howell, S. G.,
574 Huebert, B. J., Hsu, N. C., Kim, D., Kucsera, T. L., Levy, R. C.,
575 Mishchenko, M. I., Pan, X., Quinn, P. K., Schuster, G. L., Streets, D. G.,
576 Strode, S. A., Torres, O., and Zhao, X.-P. Multi-decadal aerosol variations from
577 1980 to 2009: a perspective from observations and a global model, *Atmos. Chem.*
578 *Phys.*, 14, 3657-3690, 2014.



- 579
580 11. Chu, D. A., Kaufman, Y. J., Remer, L. A., and Holben, B. N. Remote sensing of
581 smoke from MODIS airborne simulator during the SCAR-B experiment. *J.*
582 *Geophys. Res.*, 103, 31, 979–987, 1998.
583
- 584 12. Derimian, Y., Karnieli, A., Kaufman, Y. J., Andreae, M. O., Andreae, T. W.,
585 Dubovik, O., Maenhaut, W., Koren, I., and Holben, B. N. Dust and pollution
586 aerosols over the Negev desert, Israel: Properties, transport, and radiative effect. *J.*
587 *Geophys. Res.*, 111, D05205, 2006.
588
- 589 13. Dubovik, O. and King, M. D. A flexible inversion algorithm for retrieval of
590 aerosol optical properties from Sun and sky radiance measurements. *J. Geophys.*
591 *Res.*, 105 206730–20696, 2000.
592
- 593 14. Dubovik, O., Holben, B. N., Eck, T. F., Smirnov, A., Kaufman, Y. J., King, M. D.
594 Tanre, D., and Slutsker, I. Variability of absorption and optical properties of key
595 aerosol types observed in worldwide locations. *J. Atmos. Sci.*, 59, 590–608, 2002.
596
- 597 15. Dubovik, O., Sinyuk, A., Lapyonok, T., Holben, B., Mischenko, M., Yang, P., Eck,
598 T., Volten, H., Muñoz, O., Veihelmann, B., van der Zande, W. J., Leon, J.-F.,
599 Sorokin, M., and Slutsker, I. The application of spheroid models to account for
600 aerosol particle non-sphericity in remote sensing of desert dust. *J. Geophys. Res.*,
601 111, D11208, 2006.
602
- 603 16. Eck, T., Holben, B. N., Reid, J. S., O'Neill, N. T., Schafer, J. S., Dubovik, O.,
604 Smirnov, A., Yamasoe, M. A., and Artaxo, P. High aerosol optical depth biomass
605 burning events: A comparison of optical properties for different source regions,
606 *Geophys. Res. Lett.*, 200b, 30, 2035, 2003b.
607
- 608 17. Eck, T., et al. Climatological aspects of the optical properties of fine/coarse mode
609 aerosol mixtures. *J. Geophys. Res.*, 115, D19205, 2010.
610
- 611 18. Elagib, N., Addin Abdu A. Climate variability and aridity in Bahrain. *J. Arid*
612 *Environ.*, 36:405–419, 1997.
613
- 614 19. El-Askary H., Farouk R., Ichoku C., and Kafatos M. Inter-continental transport of
615 dust and pollution aerosols across Alexandria, Egypt, *Annales Geophysicae*, 27,
616 2869–2879, 2009.
617
- 618 20. Farahat, A., El-Askary, H., and Al-Shaibani, A. Study of Aerosols' Characteristics
619 and Dynamics over the Kingdom of Saudi Arabia using a Multi Sensor Approach
620 Combined with Ground Observations. *Advances in Meteorology*, Article ID
621 247531, 2015.
622
- 623 21. Farahat, A. Air Pollution in Arabian Peninsula (Saudi Arabia, United Arab
624 Emirates, Kuwait, Qatar, Bahrain, and Oman): Causes, Effects and Aerosol
625 Categorization. *Arab J of Geosci.*, 9, 196, 2016.
626



- 627 22. Farahat, A., El-Askary, H., and Dogan, A. U., 2016: Aerosols size distribution
628 characteristics and role of precipitation during dust storm formation over Saudi
629 Arabia. *Aerosol Air Qual. Res.*, 16, 2523-2534, 2016.
630
- 631 23. Farahat, A., El-Askary, H., Adetokunbo, P., Abu-Tharr, F. Analysis of aerosol
632 absorption properties and transport over North Africa and the Middle East using
633 AERONET data. *Annales Geophysicae.*, 34:11, 1031-1044, 2016.
634
- 635 24. He, Q., Li, C., Tang, X., Li, H., Geng, F., Wu, Y. Validation of MODIS derived
636 aerosol optical depth over the Yangtze River Delta in China. *Remote Sensing*
637 *Environ.*, 114, w21649–61, 2010.
- 638
- 639 25. Higurashi, A., and Nakjima, T. Development of a two-channel aerosol retrieval
640 algorithm on a global scale using NOAA AVHRR. *J. Atmos. Sci.*, 56, 924–941,
641 1999.
- 642
- 643 26. Holben, B., Eck, T., Slutsker, I., Tanre, D., Buis, J., Setzer, A. et al. AERONET—
644 A federated instrument network and data archive for aerosol characterization.
645 *Remote Sensing Environ.*, 66, 1–16, 1998.
646
- 647 27. Holben, B., Smirnov, A., Eck, T., Slutsker, I., Abuhassan, N., Newcomb, W., et al.
648 An emerging ground-based aerosol climatology—Aerosol optical depth from
649 AERONET, *J. Geophys Res.*, 106, 12067–97, 2001.
650
- 651 28. Hoell, A., Funk, C., and Barlow, M. The regional forcing of Northern Hemisphere
652 drought during recent warm tropical west Pacific Ocean La Niña events. *Clim.*
653 *Dyn.*, 42, 3289–3311, 2013.
654
655
- 656 29. Hsu, N., Gautam, R., Sayer, A., Bettenhausen, C., Li, C., Jeong, M., Tsay, S., and
657 Holben, B. Global and regional trends of aerosol optical depth over land and
658 ocean using SeaWiFS measurements from 1997 to 2012. *Atmos. Chem. Phys.*, 12,
659 8037–8053, 2012.
660
- 661 30. Ichoku, C., Chu, D. A., Mattoo, S., Kaufman, Y. J., Remer, L. A., Tanre, D.,
662 Slutsker, I., and Holben, B. N. A spatio-temporal approach for global validation
663 and analysis of MODIS aerosol product, *Geophys. Res. Lett.*, 29, 12, 8006, 2002.
664
- 665 31. Ginoux, P., Chin, M., Tegen, I., Prospero, J., Holben, B., Dubovik, O., and Lin,
666 S.-J. Sources and global distributions of dust aerosols simulated with the
667 GOCART model, *J. Geophys. Res.*, 106, 20255 – 20273, 2001.
668
- 669 32. Kahn, R. A., Gaitley, B. J., Martonchik, J. V., Diner, D. J., Crean, K. A. and
670 Holben, B. Multiangle ImagingSpectroradiometer (MISR) global aerosol optical
671 depth validation based on 2 years of coincident Aerosol Robotic Network
672 (AERONET) observations, *J. Geophys. Res.*, 110, 2005.
673
- 674 33. Kahn, R., Garay, M., Nelson, D., Yau, K., Bull, M., Gaitley, B. et al. Satellite-
675 derived aerosol optical depth over dark water from MISR and MODIS:



- 676 Comparisons with AERONET and implications for climatological studies. *J.*
677 *Geophys. Res.*, 112, D18205, 2007.
- 678
- 679 34. Kahn, R., Nelson, D., Garay, M., Levy, R., Bull, M., Diner, D., et al. MISR
680 aerosol product attributes, and statistical comparisons with MODIS. *IEEE Trans*
681 *Geosci Remote Sensing*, 47, 4095–114, 2009.
- 682
- 683 35. Kim, D., Chin, M., Bian, H., Tan, Q., Brown, M. E., Zheng, T., You, R., Diehl,
684 T., Ginoux, P., and Kucsera, T. The effect of the dynamic surface bareness on
685 dust source function, emission, and distribution, *J. Geophys. Res.*, 118, 1–16,
686 2013.
- 687
- 688 36. Kaufman, Y., Tanre, D., Remer, L., Vermote, E., Chu, A., and Holben, B.
689 Operational remote sensing of tropospheric aerosol over land from EOS moderate
690 resolution imaging spectroradiometer. *J. Geophys. Res.-Atmos.*, 102, D14,
691 17051–17067, 1997.
- 692
- 693 37. Kokhanovsky, A., Breon, F., Cacciari, A., Carboni, E., Diner, D., Di
694 Nicolantonio, W. et al. Aerosol remote sensing over land: a comparison of
695 satellite retrievals using different algorithms and instruments. *Atmos Res.*, 85,
696 372–94, 2007.
- 697
- 698 38. Liu, L., Mishchenko, M. Toward unified satellite climatology of aerosol
699 properties: direct comparisons of advanced level 2 aerosol products. *JQSRT.*, 109,
700 2376–85, 2008.
- 701
- 702 39. Marey, H., Gille, J., El-Askary, H., Shalaby, E., and El-Raey, M. Study of the
703 formation of the “black cloud and its dynamics over Cairo, Egypt, using MODIS
704 and MISR sensors. *J. Geophys. Res.*, 115, D21206, 2010.
- 705
- 706 40. Martonchik, J., Diner, D., Crean, K., and Bull, M. Regional aerosol retrieval
707 results from MISR. *IEEE Trans. Geosci. Remote Sens.*, 40, 1,520–1,531, 2002.
- 708
- 709 41. Mishchenko, M., I. Geogdzhayev, L. Liu, A. Lacis, B. Cairns, L. Travis. Toward
710 unified satellite climatology of aerosol properties: what do fully compatible
711 MODIS and MISR aerosol pixels tell us? *J Quant Spectrosc Radiat Transfer.* 110,
712 402–8, 2009.
- 713
- 714 42. Mishchenko, M., Liu, L., Geogdzhayev, I., Travis, L., Cairns, B., Lacis, A.
715 Toward unified satellite climatology of aerosol properties: 3. MODIS versus
716 MISR versus AERONET. *J Quant Spectrosc Radiat Transfer.*, 111, 540–52, 2010.
- 717
- 718 43. Remer, L., Kaufman, Y., Tanre, D., Mattoo, S., Chu, D., Martins, J., et al. The MODIS
719 aerosol algorithm, products, and validation. *J Atmos Sci.*, 62, 947–73, 2005.
- 720
- 721 44. Sadiq, M. and McCain, J. *The Gulf War Aftermath: An Environmental Tragedy.*,
722 1st ed., Springer, 1993.
- 723
- 724 45. Sayer, A., Hsu, N., Eck, T., Smirnov, A., and Holben, B. AERONET-based
725 models of smoke-dominated aerosol near source regions and transported over



- 726 oceans, and implications for satellite retrievals of aerosol optical depth. *Atmos.*
727 *Chem. Phys.*, 14, 11493-11523, 2014.
728
- 729 46. Schepanski, K., Mallet, M., Heinold, B., and Ulrich, M.: North African dust
730 transport toward the western Mediterranean basin: atmospheric controls on dust
731 source activation and transport pathways during June–July 2013, *Atmos. Chem.*
732 *Phys.*, 16, 14147-14168, 2016.
733
- 734 47. Sioris, C. E., McLinden, C. A., Shephard, M. W., Fioletov, V. E., and Abboud, I.:
735 Assessment of the aerosol optical depths measured by satellite-based passive
736 remote sensors in the Alberta oil sands region, *Atmos. Chem. Phys.*, 1931-1943,
737 2017.
738
- 739 48. Smirnov, A., Holben, B., Eck, T., Dubovik, O., and Slutsker, I. Cloud-screening
740 and quality control algorithms for the AERONET data-base, *Remote Sens.*
741 *Environ.*, 73, 337 – 349, 2000.
742
- 743 49. Solomos, S., Ansmann, A., Mamouri, R.-E., Biniatoglou, I., Patlakas, P.,
744 Marinou, E., and Amiridis, V. Remote sensing and modelling analysis of the
745 extreme dust storm hitting the Middle East and eastern Mediterranean in
746 September 2015, *Atmos. Chem. Phys.*, 17, 4063-4079, 2017.
- 747
- 748 50. Todd M., R. Washington, Vanderlei, M., Dubovik, O., Lizcano, G., M'Bainayel,
749 S., Engelstaedter, S. Mineral dust emission from the Bodélé Depression, northern
750 Chad, during BoDEx 2005. *J. Geophys. Res.*, 112, D06207, 2007.
751
- 752 51. Von Hoyningen-Huene, W., Posse, P. Nonsphericity of aerosol particles and their
753 contribution to radiative forcing. *JQSRT*, 57, 651–68, 1997.
754
755
- 756 52. Yu, Y., Notaro, M., Liu, Z., Kalashnikova, O., Alkolibi, F., Fadda, E., and
757 Bakhrjy, F. Assessing temporal and spatial variations in atmospheric dust over
758 Saudi Arabia through satellite, radiometric, and station data, *J. Geophys. Res.*
759 *Atmos.*, 118, 13, 253–13, 264, 2013.
760
- 761 53. Yu, Y., Notaro, M., Liu, Z., Wang, F., Alkolibi, F., Fadda, E. and Bakhrjy,
762 F. Climatic controls on the interannual to decadal variability in Saudi Arabian
763 dust activity: Toward the development of a seasonal dust prediction model. *J.*
764 *Geophys. Res. Atmos.*, 120, 1739–1758, 2015.
765
- 766 54. Zhao, G. and Girolamo, L. A cloud fraction versus view angle technique for
767 automatic in-scene evaluation of the MISR cloud mask. *J. Appl. Meteorol.*, 43, 6,
768 860–869, 2004.
- 769
- 770
- 771



772

773

774

775

776

777 **Tables' caption**

778 Table 1. Geographic location of the AERONET sites used in this study

779 Table 2. Statistics for dust sites, R: correlation coefficient, RMSE: Root Mean Square
780 deviation; G-fraction: good fraction; N: number of observations

781 Table 3. Statistics for biomass and mixed sites, parameters as in Table 3. Caption.

782 Table 4. MISR coverage for six days of major dust activity over the Arabian Peninsula
783 during March 2009.

784

785

786

787

788

789

790

791

792

793

794

795

796



797

798

799 **Figures caption**

800 Figure 1. Location of the AERONET stations over North Africa and the Middle East. The
801 numbers on the map indicates the site location as 1: Saada, 2: Tamanrasset_INM, 3: Cairo,
802 4: Sede Boker, 5: Solar Village, 6: Mezaira, 7: Bahrain.

803 Figure 2. Scatter plot of MISR AOD versus AERONET AOD based on seasons and
804 aerosols categorization.

805 Figure 3. Scatter plot of MODIS AOD versus AERONET AOD based on seasons and
806 aerosols categorization.

807 Figure 4. Time series of monthly mean AOD derived from MODIS/Aqua, MODIS/Terra,
808 MISR and AERONET over a) dust b) biomass and c) mixed dominated aerosol regions.

809 Figure 5. Long range AOD difference for MODIS/Terra and MODIS/Aqua over the dust,
810 biomass and mixed sites.

811 Figure 6. Histogram of the MISR, MODIS and Solar Village AERONET measurements a)
812 MISR b) MODIS data retrievals.

813 Figure 7. Histogram of the MISR, MODIS and Mezaria AERONET measurements a)
814 MISR b) MODIS data retrievals.

815 Figure 8. Histogram of the MISR, MODIS and Bahrain AERONET measurements a) MISR
816 b) MODIS data retrievals.

817 Figure 9. Histogram of the MISR, MODIS and SAADA AERONET measurements a)
818 MISR b) MODIS data retrievals.

819 Figure 10. Histogram of the MISR, MODIS and Taman AERONET measurements a)
820 MISR b) MODIS data retrievals.



821 Figure 11. Histogram of the MISR, MODIS and SEDEE Boker AERONET measurements

822 a) MISR b) MODIS data retrievals.

823 Figure 12. Histogram of the MISR, MODIS and Cairo AERONET measurements a) MISR

824 b) MODIS data retrievals.

825

826

827

828

829

830

831

832

833

834

835

836

837

838

839

840

841

842

843

844

845



846

847

848

Table 1.

Location name	Lon./Lat.	Measurement period
Solar Village	24.907° N/46.397° E	2000-2015
Mezaria	23.105° N/53.755° E	2004-2015
Bahrain	26.208° N/50.609° E	2000-2006
Saada	31.626° N/8.156° W	2003-2015
Taman	22.790° N/5.530° E	2000-2015
Cairo	30.081° N/31.290° E	2005 -2007
Sede Boker	30.855° N/34.782 ° E	2000-2015

849

850

851

852

853

854

855

856

857

858

859

860

861

862

863



864

Table 2.

AERONET	Sensor	Season	Mean Value	N	R	Gfraction (%)	
Site							
			AERONET				
			Satellite				
		DJF	0.31±0.22	0.38±0.20	338	0.94	60.05
		MAM	0.39±0.27	0.45±0.23	89	0.94	65.16
	MISR	JJA	0.39±0.18	0.45±0.17	141	0.90	70.21
		SON	0.27±0.16	0.35±0.14	3	0.99	33.33
Solar Village		DJF	0.27±0.19	0.33±0.17	1500	0.48	51.80
		MAM	0.36±0.24	0.26±0.17	389	0.68	90.23
	MODIS	JJA	0.34±0.17	0.42±0.19	429	0.41	54.31
	Terra	SON	0.22±0.10	0.36±0.12	471	0.51	28.87
		DJF	0.33±0.15	0.40±0.17	60	0.89	75.00
		MAM	0.32±0.19	0.41±0.22	13	0.90	69.23
	MISR	JJA	0.42±0.13	0.47±0.17	21	0.85	80.95
		SON	0.29±0.07	0.36±0.07	22	0.87	77.27
Mezaria		DJF	0.32±0.15	0.35±0.19	198	0.86	74.74
		MAM	0.44±0.33	0.45±0.27	115	0.92	78.07
	MODIS	JJA	0.39±0.14	0.43±0.20	89	0.81	71.91
	Terra	SON	0.28±0.13	0.30±0.16	97	0.87	77.31
		DJF	0.37±0.11	0.31±0.10	17	0.73	100
		MAM	0.31±0.11	0.28±0.14	3	0.89	100
	MISR	JJA	0.40±0.09	0.36±0.09	8	0.69	100
		SON	0.40±0.09	0.30±0.05	4	0.98	100
Bahrain		DJF	0.42±0.29	0.20±0.19	121	0.41	93.38
		MAM	0.50±0.28	0.13±0.15	25	0.26	96.00
	MODIS	JJA	0.55±0.26	0.31±0.27	42	0.50	88.09
	Terra	SON	0.35±0.14	0.21±0.12	29	0.32	93.10

865

866

867
868

Table 3.

AERONET	Method	Season	Mean Value	N	R	Gfraction	
Site						(%)	
			AERONET	Satellite			
SAADA	MISR	DJF	0.24±0.16	0.22±0.15	149	0.93	97.29
		MAM	0.21±0.13	0.19±0.11	53	0.89	96.15
		JJA	0.29±0.14	0.27±0.15	80	0.93	97.46
		SON	0.19±0.15	0.19±0.12	60	0.94	98.30
	MODIS Terra	DJF	0.23±0.16	0.32±0.21	550	0.57	57.81
		MAM	0.24±0.18	0.39±0.23	90	0.43	44.44
		JJA	0.30±0.17	0.45±0.18	201	0.40	45.27
		SON	0.19±0.13	0.22±0.14	162	0.71	72.39
Taman	MISR	DJF	0.19±0.23	0.24±0.19	135	0.92	70.89
		MAM	0.29±0.22	0.35±0.24	24	0.97	82.60
		JJA	0.35±0.30	0.39±0.19	36	0.85	71.42
		SON	0.19±0.15	0.19±0.12	60	0.94	98.30
	MODIS Terra	DJF	0.19±0.22	0.18±0.16	319	0.67	81.81
		MAM	0.24±0.19	0.22±0.17	67	0.55	83.58
		JJA	0.37±0.32	0.29±0.20	69	0.69	84.05
		SON	0.14±0.14	0.13±0.10	117	0.54	84.61
Cairo	MISR	DJF	0.33±0.20	0.28±0.11	13	0.94	100
		MAM	0.22±0.06	0.24±0.08	5	0.99	100
		JJA	0.43±0.23	0.34±0.11	5	0.99	100
		SON	0.38±0.21	0.29±0.12	4	0.97	100
	MODIS Terra	DJF	0.33±0.16	0.20±0.11	158	0.30	95.56
		MAM	0.32±0.16	0.12±0.08	39	0.25	100
		JJA	0.35±0.14	0.28±0.07	58	0.17	94.82
		SON	0.38±0.19	0.20±0.09	29	0.07	93.82
		DJF	0.14±0.06	0.21±0.07	23	0.87	40.90



	MAM	0.14±0.05	0.24±0.09	13	0.68	33.33
MISR	JJA	0.16±0.05	0.24±0.06	163	0.85	33.33
	SON	0.15±0.07	0.23±0.06	72	0.89	33.80
SEDEE_BOKER	DJF	0.16±0.12	0.23±0.14	1312	0.36	53.50
	MAM	0.21±0.18	0.24±0.19	338	0.34	65.68
MODIS	JJA	0.16±0.09	0.33±0.13	392	0.27	17.34
	Terra	SON	0.16±0.09	0.23±0.12	477	0.46

869

870

871

872

873

874

875

876

877

878

879

880

881

882

883

884

885

886

887



888

Table 4.

	AERONET		MISR		MODIS	
	AOD		AOD		AOD	
	N	% > 0.4	N	% > 0.4	N	% > 0.4
Solar	3978	28.7	684	32.8	2789	30.1
Village						
Mezaria	1650	30.2	547	45.7	498	40.7
Bahrain	1117	33.3	676	35.7	217	18.4
SAADA	3184	10.8	667	11.5	1004	34.6
Taman	1863	17.9	845	22.6	572	9.4
Cairo	269	53.5	620	17.7	284	4.2
SEDEE	5722	4.8	675	9	2519	12.8

889

890

891

892

893

894

895

896

897

898

899

900

901

902



903

904

905

906

907

908

909

910

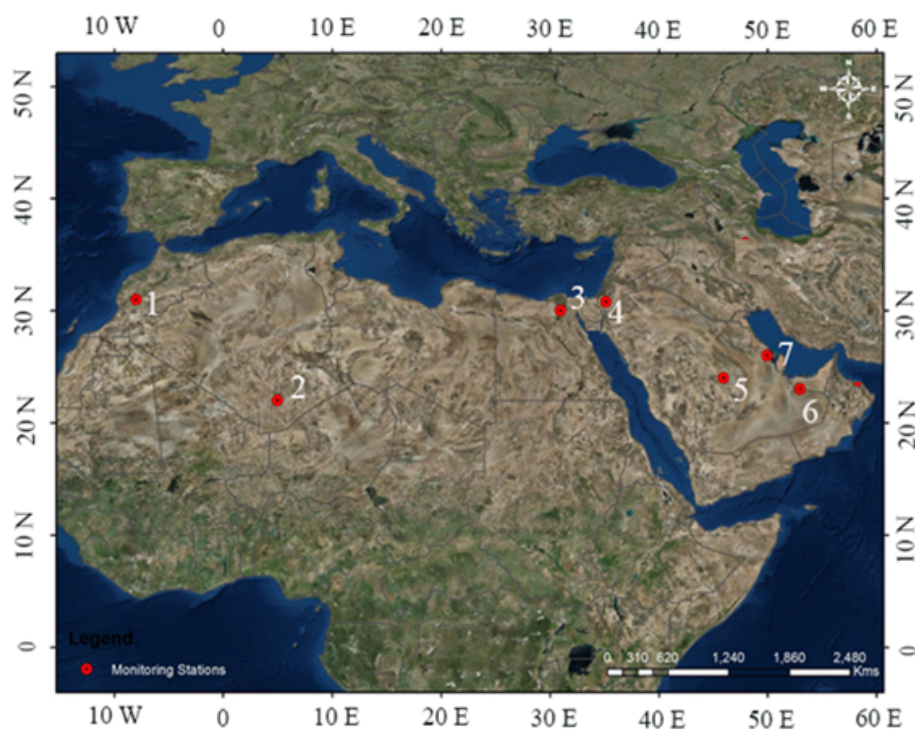
911

912

913

914

915



916 Figure 1.

917

918

919

920

921

922

923

924

925

926

927



928

929

930

931

932

933

934

935

936

937

938

939

940

941

942

943

944

945

946

947

948

949

950

951

952

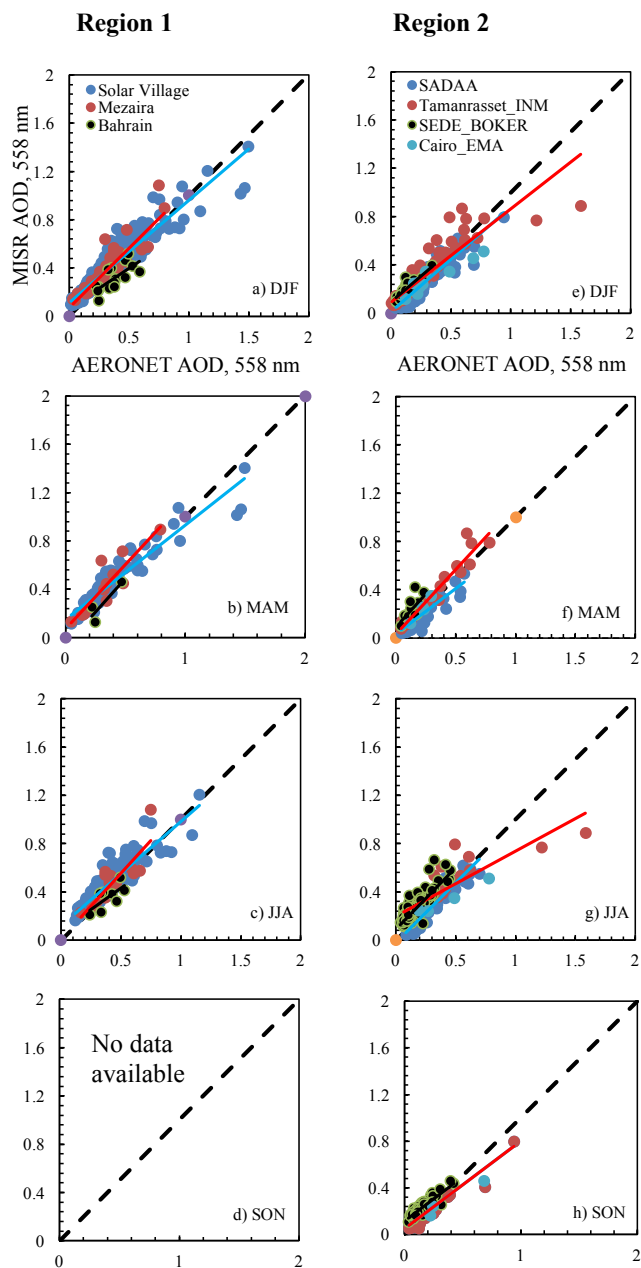


Figure 2.



953

954

955

956

957

958

959

960

961

962

963

964

965

966

967

968

969

970

971

972

973

974

975

976

977

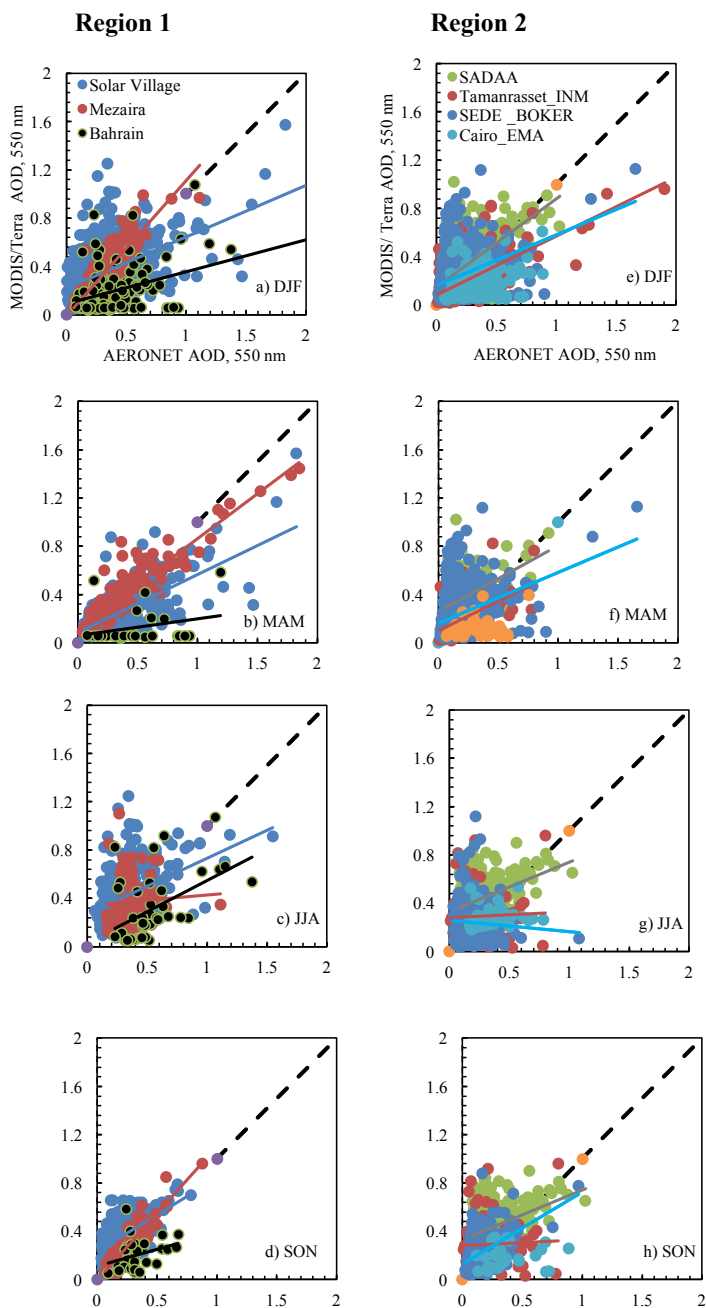


Figure 3.



978

979

980

981

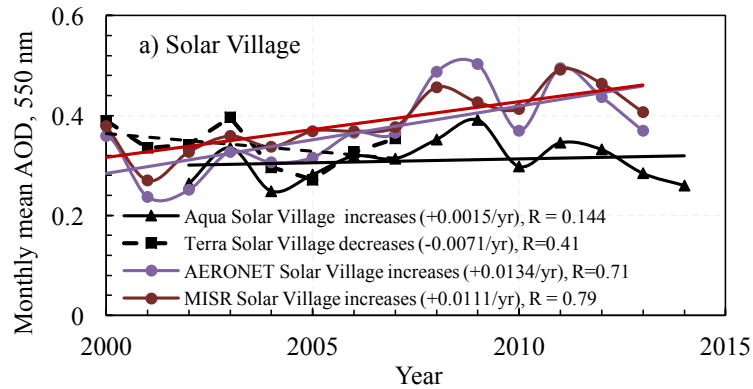
982

983

984

985

986



987

988

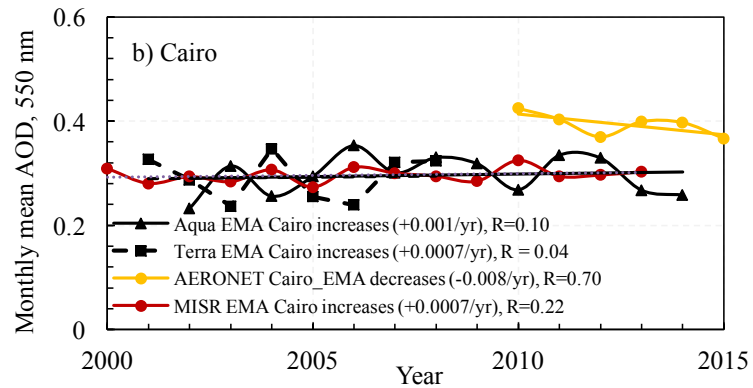
989

990

991

992

993



994

995

996

997

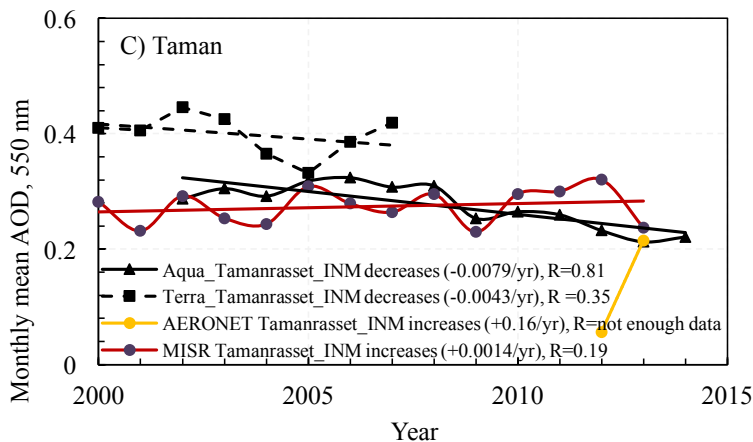
998

999

1000

1001

1002





1003 Figure 4.

1004

1005

1006

1007

1008

1009

1010

1011

1012

1013

1014 Figure 5.

1015

1016

1017

1018

1019

1020

1021

1022

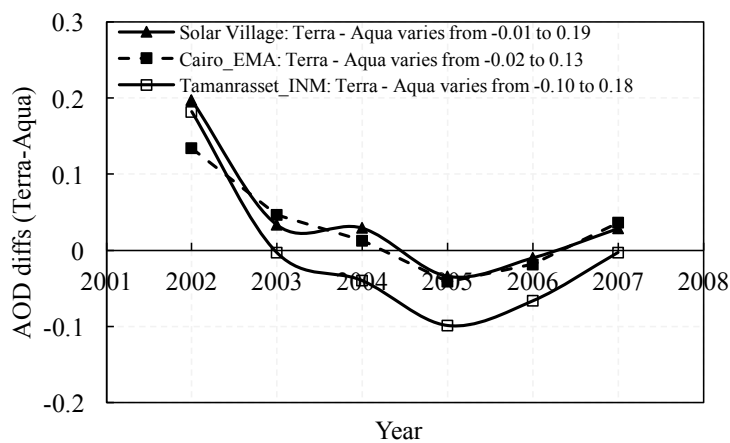
1023

1024

1025

1026

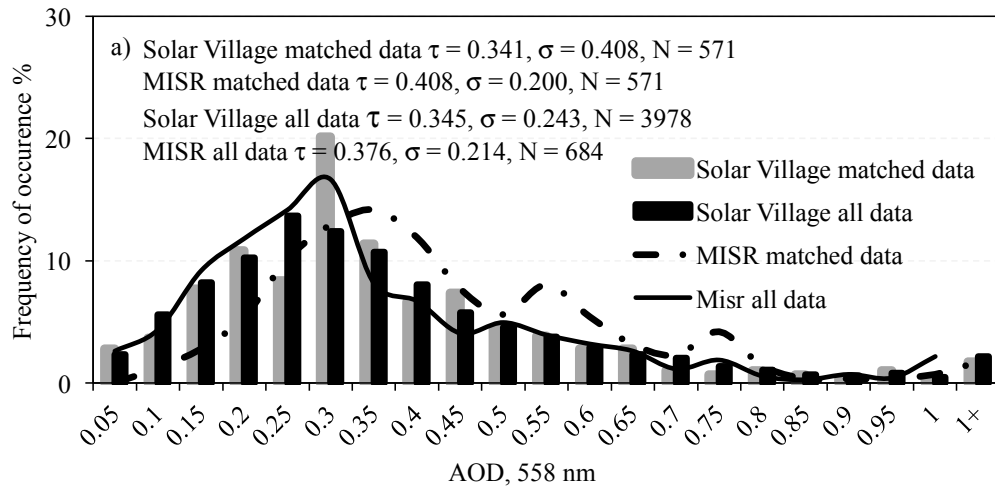
1027



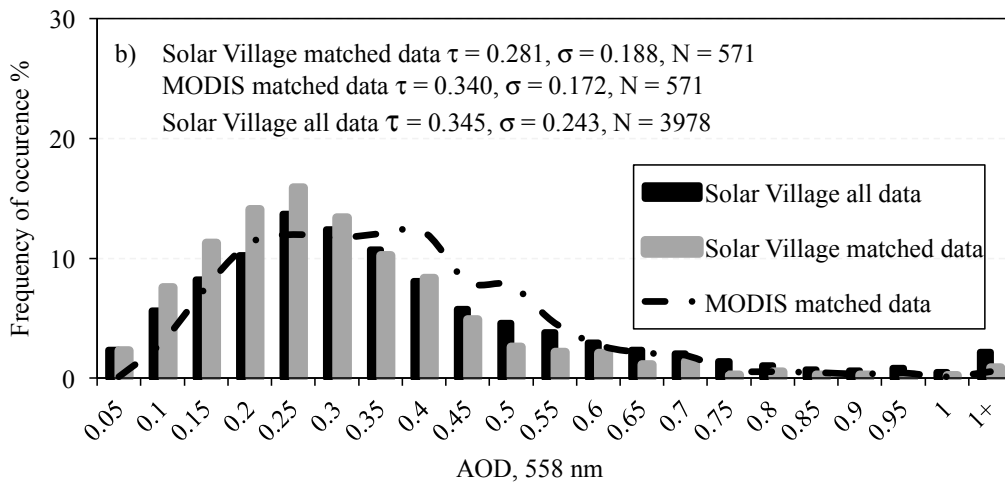


1028

1029



1030



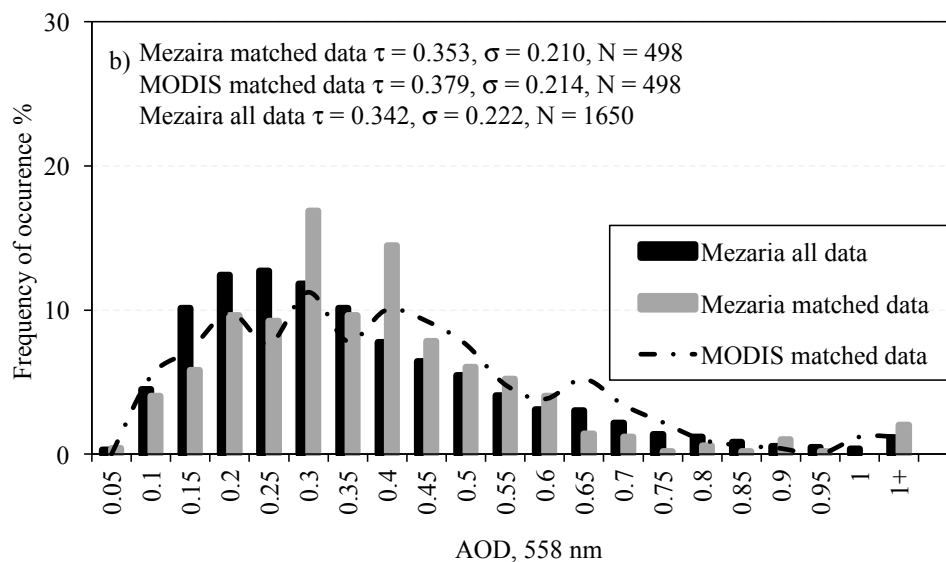
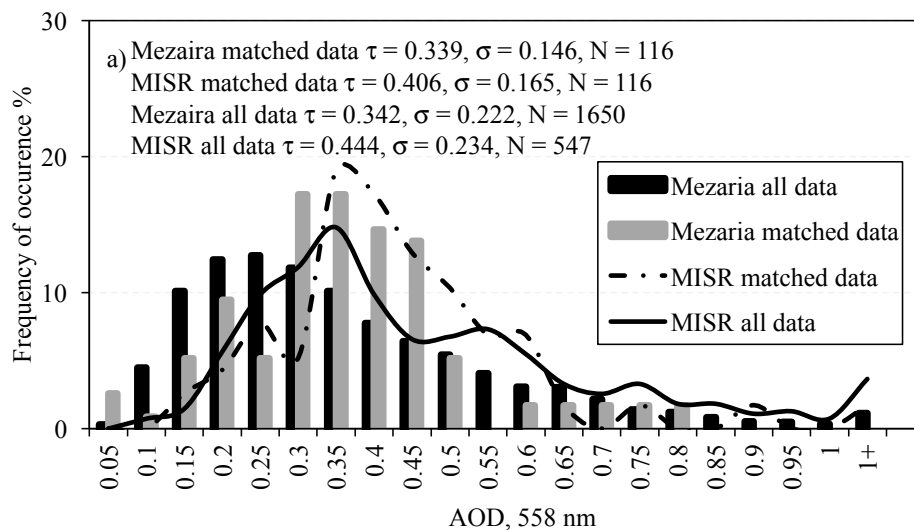
1031

1032 Figure 6.

1033

1034

1035



1036

1037

1038

1039

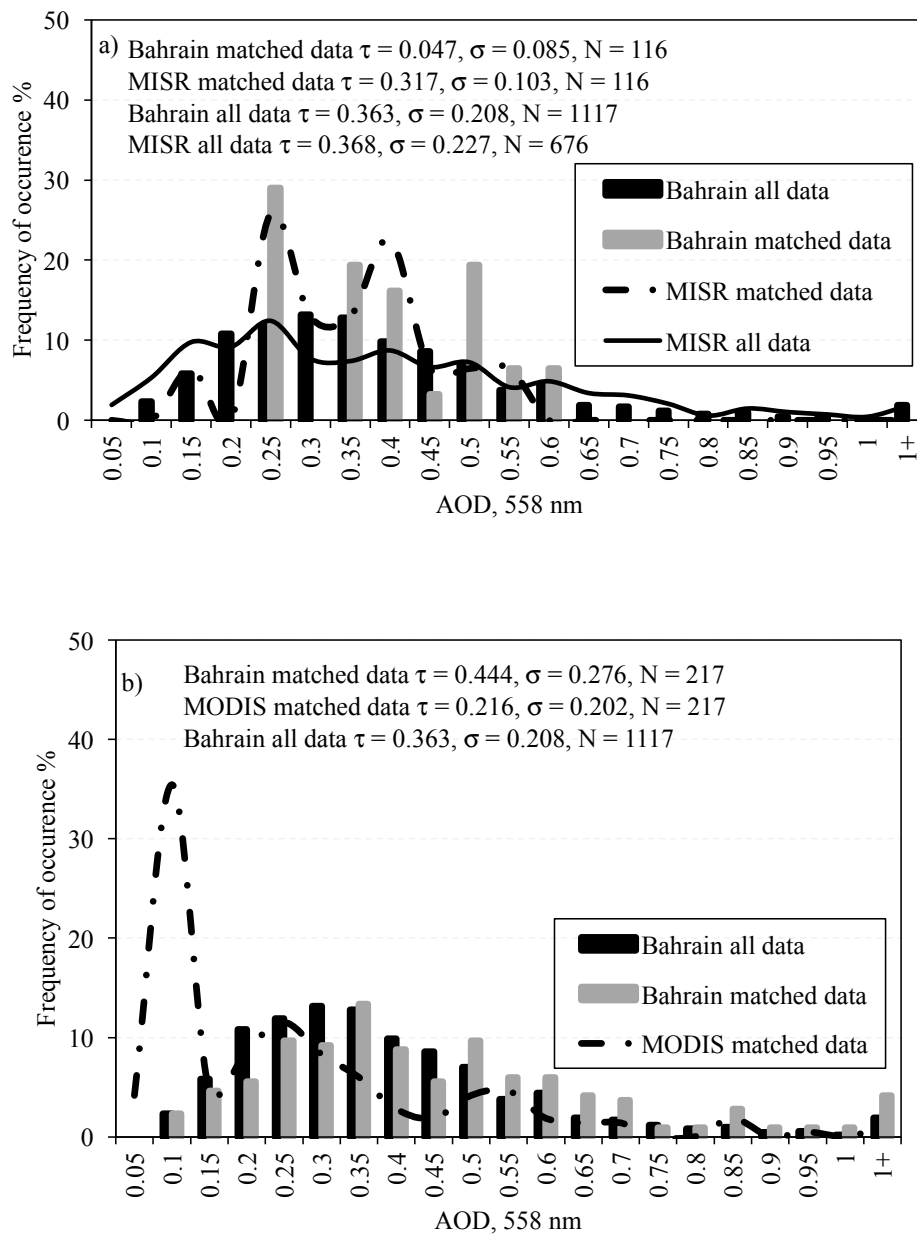
Figure 7.

1040

1041



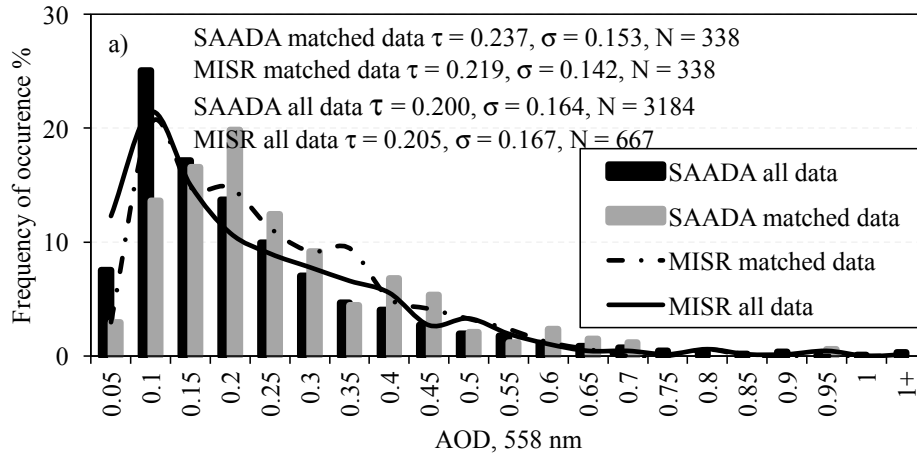
1042



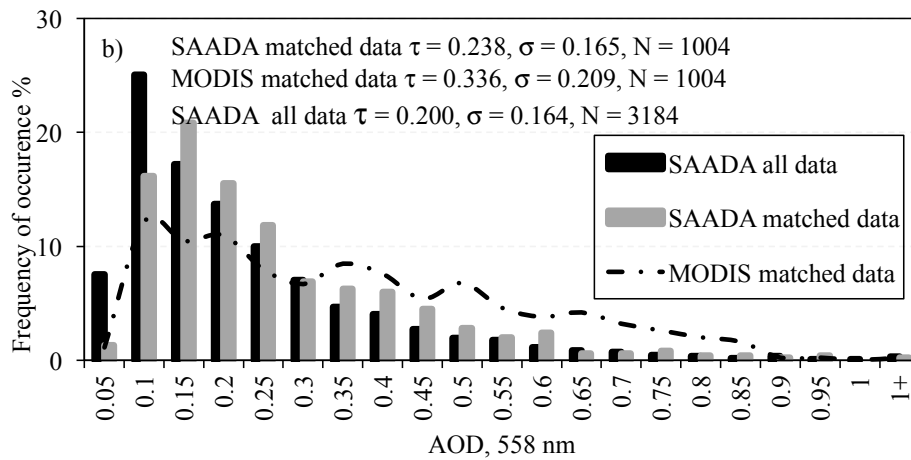
1043 Figure 8.



1044



1045



1046

1047

1048 Figure 9.

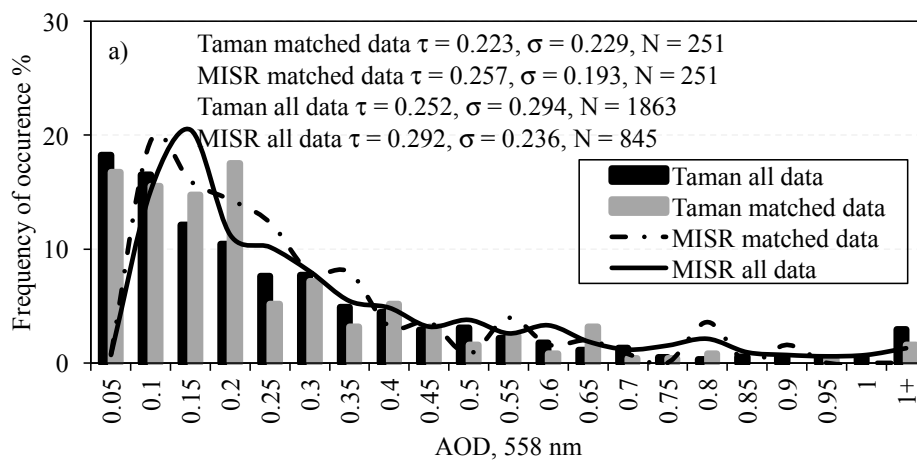
1049

1050

1051

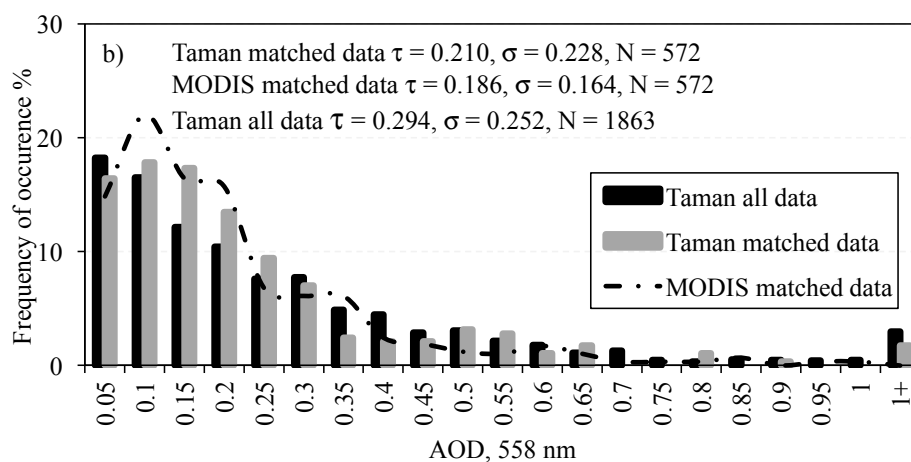


1052



1053

1054



1055

1056

1057

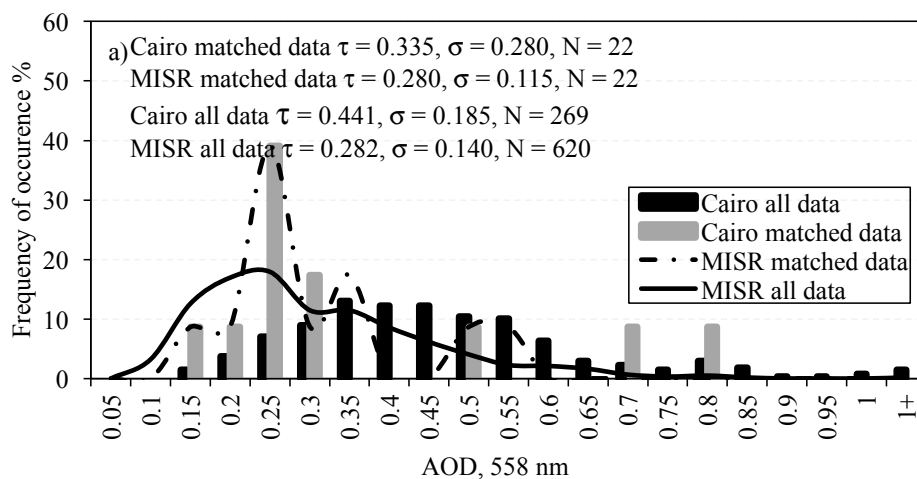
1058 Figure 10.

1059

1060

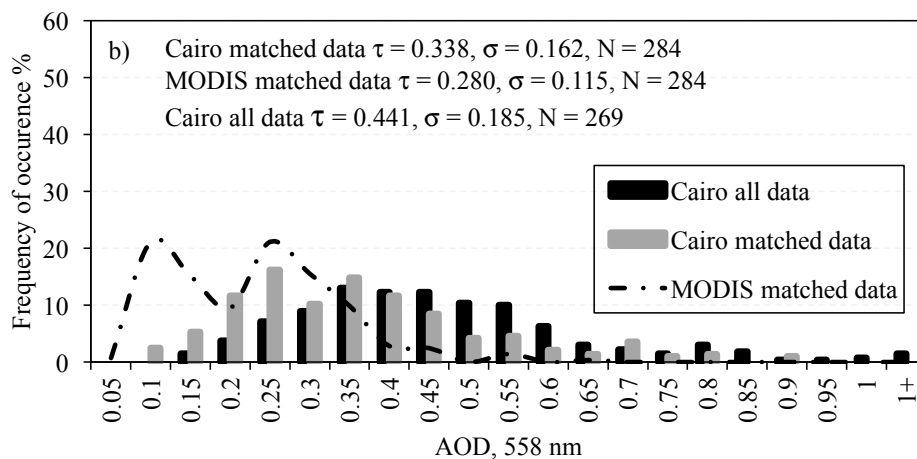


1061



1062

1063



1064

1065

1066

1067

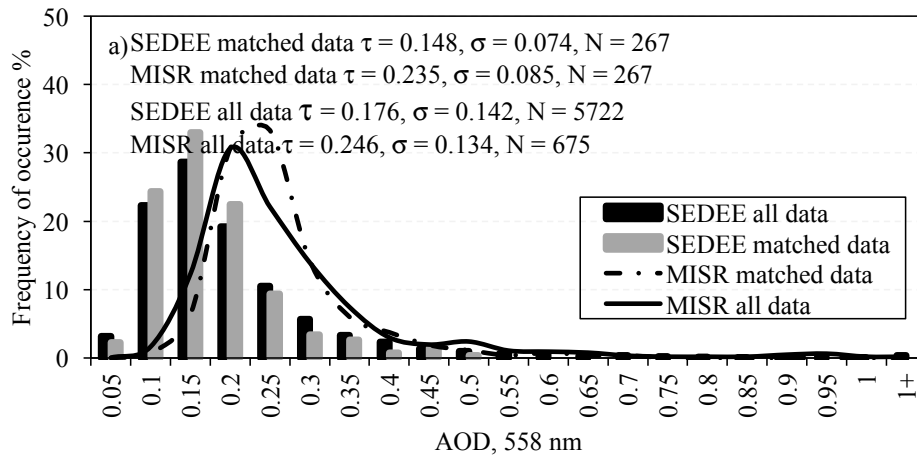
1068 Figure 11.



1069

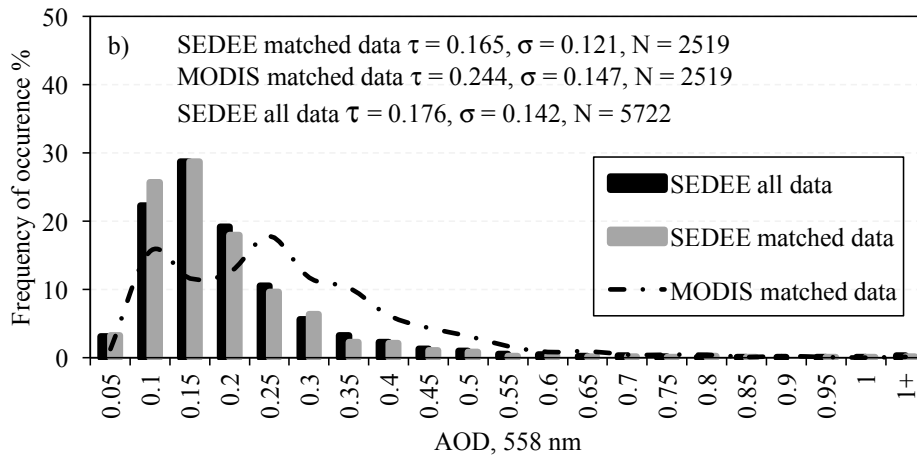
1070

1071



1072

1073



1074

1075

1076 Figure 12.